Journal of Hydrology 409 (2011) 350–362

Contents lists available at SciVerse ScienceDirect

Journal of Hydrology

journal homepage: www.elsevier.com/locate/jhydrol

Hydraulic tomography analog outcrop study: Combining travel time and steady shape inversion

R. Hu [a,*], R. Brauchler [b], M. Herold [a], P. Bayer [b]

[a] Geoscience Center, University of Göttingen, Goldschmidtstraße 3, 37077 Göttingen, Germany
[b] Federal Institute of Technology ETH Zurich, Department of Earth Sciences, Sonneggstrasse 5, 8092 Zurich, Switzerland

ARTICLE INFO

Article history:
Received 28 December 2010
Received in revised form 2 August 2011
Accepted 11 August 2011
Available online 22 August 2011
This manuscript was handled by Philippe Baveye, Editor-in-Chief, with the assistance of Xunhong Chen, Associate Editor

Keywords:
Hydraulic tomography
Inversion strategy
Aquifer analog

SUMMARY

Travel time and steady shape inversions are complementary methods for tomographic aquifer characterization. In this work, a combined procedure is presented that facilitates determination of spatial hydraulic conductivity and specific storage distributions in heterogeneous groundwater systems. The procedure is applied to a highly heterogeneous sedimentary aquifer analog that is implemented as a two- and three-dimensional case study in a numerical flow model. By interpreting the observations from multiple simulated short-term pumping tests, the main hydraulic features of the analog are successfully reconstructed. The final results demonstrate the encouraging potential of the combined procedure for identifying the dominant structural elements and composition of sedimentary aquifers. However, limits derived from the test design of hydraulic travel time tomography in our synthetic case study prevented us from resolving small scale (10 cm in size) variability of hydraulic conductivity with high discrepancies (up to 5 orders of magnitude). A better reconstruction of the aquifer hydraulic parameters is expected by utilizing a larger amount of measurements, which involve more test and observation intervals, although such a test design would be less feasible for field applications. Still, this newly combined scheme is very attractive for an up-scaled reconstruction on the sub-meter scale. For the present case study, representative parameter values could be estimated in a computationally efficient way.

1. Introduction

The mapping of hydraulic subsurface features, as well as their property estimation and process monitoring, is essential for rigorous analysis of a variety of engineering, geotechnical and hydrogeological problems within the context of water resources management (Rubin and Hubbard, 2005). Especially the prediction of contaminant transport strongly depends on the accuracy of hydraulic description (Zheng and Gorelick, 2003; Maier et al., 2009). Hence, it is important to develop investigation methods which allow the characterization of hydraulic subsurface properties, for example, the continuity of preferential flow paths or the presence of hydraulic barriers (Poeter and McKenna, 1995). However, the characterization of aquifers is often insufficient to predict detailed transport processes even at well-instrumented groundwater research test sites (Butler, 2005; Teutsch et al., 1998; Farrell et al., 1994).

A new approach, termed hydraulic tomography, which has evolved from the concept of medical and geophysical tomography, has been developed over the last approximately fifteen years (e.g. Gottlieb and Dietrich, 1995; Butler et al., 1999; Bohling et al., 2002, 2007; Bohling, 2009; Bohling and Butler, 2010; Yeh and Liu, 2000; Vesselinov et al., 2001a,b; Zhu and Yeh, 2005, 2006; Liu et al., 2002, 2007; Illman et al., 2008, 2009, 2010; Yin and Illman, 2009; Fienen et al., 2008; Li et al., 2007, 2008; Cardiff et al., 2009). This approach shows a great potential for reconstructing detailed spatial distributions of hydraulic parameters between wells. Hydraulic tomography utilizes a series of hydraulic cross-well interference tests, whereby the wells are separated into hydraulically isolated sections by means of packer systems or a multi-chamber design. By varying pumping (or injection) intervals and observation intervals between the tests, a hydraulic tomographic data set of a large number of transient pressure responses can be recorded. Ultimately, by applying an appropriate inverse model to fit the pressure responses or parts of them, a detailed two- or three-dimensional reconstruction image that reflects the hydraulic heterogeneity between wells can be derived. Thereby the forward step of the inversion, i.e. the solution of the stationary or transient groundwater flow equation, is obtained by a numerical flow model and the inverse step is performed by a parameter estimator.

An alternative inversion approach, which has successfully been applied in several studies, is based on the inversion of travel times of a transient pressure response by solving the eikonal equation instead of the groundwater flow equation (e.g. Vasco et al., 2000; Vasco and Karasaki, 2006; Kulkarni et al., 2000; Datta-Gupta

* Corresponding author.
E-mail address: rhu@gwdg.de (R. Hu).

0022-1694/$ - see front matter © 2011 Elsevier B.V. All rights reserved.
doi:10.1016/j.jhydrol.2011.08.031

et al., 2001; Brauchler et al., 2003, 2007, 2010, 2011; He et al., 2006). This approach follows the procedure of seismic ray tomography. A travel time integral relates the square root of the peak travel time of the transient pressure pulse to the inverse square root of the hydraulic diffusivity for a Dirac point source at the origin. Thereby, diffusivity is defined as the quotient of hydraulic conductivity over storage and provides a quantitative measure for the rate of response during transient flow. The derivation of the travel time integral is based on the transformation of the transient groundwater flow equation into an eikonal equation using an asymptotic approach (Virieux et al., 1994). The eikonal equation can be solved with ray tracing techniques, which facilitate the calculation of pressure propagation along trajectories. Ray tracing techniques are computationally very efficient and allow the inversion of hundreds of travel times derived from hydraulic cross-well short term tests within a few seconds using a personal computer. However, the computational efficiency of ray tracing techniques is offset to some degree by the time involved in the pre-processing of the data and the results could be influenced by uncertainty when picking travel times from the field data. Moreover, this method estimates only the diffusivity, neglecting the separate importance of the diffusivity components, which are hydraulic conductivity and specific storage.

The steady shape analysis of tomographic pumping tests, proposed by Bohling et al. (2002, 2007), is an attractive complementary method to the above mentioned travel time inversion. At steady shape conditions, drawdown varies with time but the hydraulic gradient does not. Jacob (1963) and Kruseman and de Ridder (1990) describe the steady-shape flow regime as steady-radial flow and transient steady-state flow regimes, respectively. The constant hydraulic gradient is determined mainly by the pumping conditions and the conductivity distribution within the area of investigation. Steady shape conditions should be reached prior to the time when boundary conditions exert significant influence on the head response. Therefore, this method is well suited for the evaluation of a large number of hydraulic cross-well tests in a short time without significant influence from the outer boundary. The transient data can be analyzed with the computational efficiency of a steady state model to estimate hydraulic conductivity even though the flow system may be far from true steady-state conditions. Application of a steady-state model reduces the calculation time by several orders of magnitude in comparison to standard inversions of transient data.

In this study we propose a two-step inversion procedure, which is based on coupling travel time and steady shape inversion. Thereby we follow the suggestions by Bohling et al. (2007). In the first step, we utilize the computationally efficient hydraulic diffusivity tomography approach of Brauchler et al. (2003) to construct zones of constant diffusivity. In the second step, hydraulic conductivity and specific storage estimates are determined for each zone by steady shape analysis of tomographic measurements. The combined inversion scheme is tested using two- and three-dimensional numerical data sets derived from a sedimentary aquifer analog outcrop study by Bayer (1999).

2. Modeling of short term pumping tests

2.1. Aquifer analog outcrop study

Theoretical numerical studies are often a cost effective way to develop and evaluate new investigation techniques. However, transferability into practice can only be evaluated by testing in the field. Even then, the quality of measured data interpretation can hardly be assessed exactly as the true field conditions are not fully known. In order to maximize the expressiveness of numerical studies, they therefore should simulate field conditions as realistically as possible. An attractive approach is to make use of aquifer analogs. Such analogs are often derived from mapping outcrops and have mainly been used in the petroleum industry for reservoir characterization (Flint and Bryant, 1993). In particular structural and textural features can be deduced that represent the characteristics of the hardly accessible reservoir rocks. In hydrogeology, emphasis is set on outcrop analogs of complex sedimentary formations, which are of special interest due to their relevance as hosts of highly productive aquifers. Using such analogs, detailed inspection of natural heterogeneity of hydraulic properties is possible (Teutsch et al., 1998; Huggenberger and Aigner, 1999).

The data base of the numerical investigations presented in the following study, is from the aquifer analog outcrop study close by the village Herten in SW Germany performed by Bayer (1999) and published in Bayer et al. (2011). Six parallel profiles of an unconsolidated sedimentary body with a size of 16 m × 10 m × 7 m are provided. During a period of six months, the gravel quarry was excavated in a stepwise fashion as the quarry face was moved back 10 m in total. Every two meters, high resolution photographs were taken of each exposed face, yielding six parallel images. The outcrop photographs were then interpreted to yield facies maps of lithology, using observed texture, sediment grain size, and GPR (Ground Penetrating Radar) surveys. From a hydrogeological perspective, the focus is set on hydrofacies, i.e. zones of similar hydraulic conductivity and porosity. Hence, for each lithological unit, laboratory measurements for hydrofacies' classification were performed. Maji and Sudicky (2008) present a geostatistical analysis of the generated hydrofacies mosaics. Based on transition probability Markov chain geostatistics, they interpolated between the six profiles and translated the gathered information into a three-dimensional (3-D) hydraulic parameter distribution. The 3-D characterization of the aquifer analog makes the highly resolved parameter distribution unique with a resolution of 5 cm × 5 cm × 5 cm.

The Herten analog serves as a basis for the numerical groundwater model, which is utilized in the present study to simulate short term pumping tests arranged in a tomographic array. The hydrofacies-specific hydraulic conductivity values are taken from Bayer (1999) as given in Maji and Sudicky (2008). The specific storage values are taken from data reported in the literature (Domenico and Mifflin, 1965). Each main hydrofacies group is assigned a specific storage value (Table 1). For computational reasons, the analog data set is scaled up to 10 cm × 10 cm × 10 cm, which means a reduction of the total number of cells from approximately 9 million to approximately 1 million. Fig. 1 shows a 3-D image of the hydraulic conductivity and specific storage distribution. Although the resolution reduction and the rigorous definition of specific storage are a compromise between data quality and practicability, the images displayed in Fig. 1 still maintain highly resolved sedimentary structures such as small scale layering and cross-beddings, which reflect the corresponding hydrofacies distribution.

2.2. Numerical simulation of hydraulic tests

A groundwater model is set-up using MODFLOW-96 (Harbaugh and McDonald, 1996) to simulate short term pumping tests arranged in a tomographic array. The aquifer analog data set with a volume of 16 m × 10 m × 7 m is embedded in the center of the model domain on a uniform 10 cm grid. Outside of this area the mesh is telescopically coarsened and increasing cell sizes are employed, ranging from 10 cm at the central domain of interest to 100 m at the model boundaries. The distance from the center to the constant head boundary is about 600 m. The hydraulic parameters for the cells of the extended area are the

Table 1
Lithofacies, hydrofacies and their corresponding values for hydraulic conductivities (m s^{-1}) and specific storages (m^{-1}).

Lithofacies code	Characterization	Hydrofacies code	Characterization	Hydraulic conductivity (m s^{-1})	Specific storage (m^{-1})
Gcg, a	Gravel matrix free well rounded	Gcgo cGcgo sGcgo	Gravel,open framework Stone-rich gravel Stone-rich gravel(coarse)	8.0×10^{-2} 1 1.0×10^{-3}	3.62×10^{-5}
Gcm	gravel well- to rounded moderate to poor sorting	cGcm Gcm	Stone-rich gravel Sand-rich gravel	2.3×10^{-4} 2.5×10^{-4}	4.90×10^{-5}
GSx	Gravel/sand mixtures well sorted and rounded	fGcmb sGcmb sGcm GSx	Bimodal silt-gravel mixture Bimodal sand-gravel mixture Sand-rich gravel Sand/silt-gravel mixture	6.0×10^{-7} 4.3×10^{-5} 6.1×10^{-5} 1.5×10^{-4}	1.02×10^{-4}
S-x	Sand	S-x	Pure sand accumulation	8.0×10^{-4}	2.00×10^{-4}

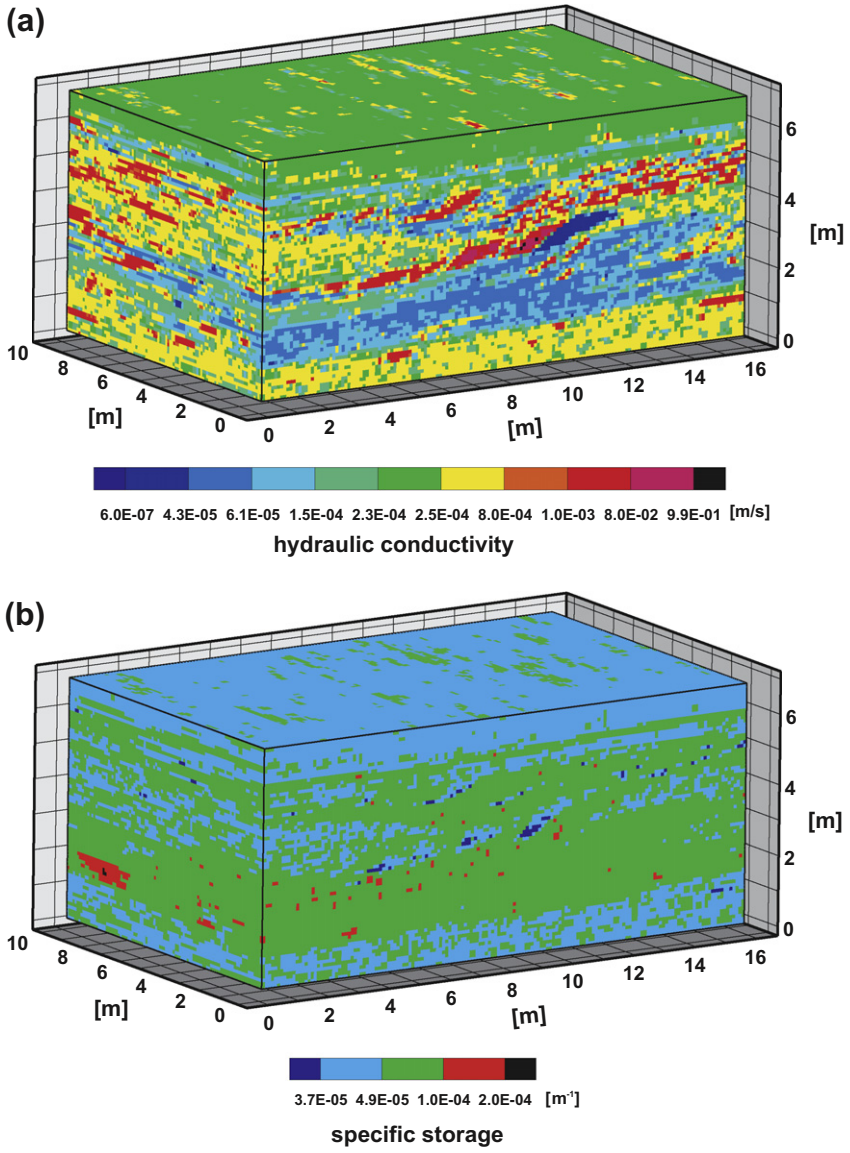

Fig. 1. Three-dimensional (3-D) images of the up-scaled hydraulic conductivity (a) and specific storage distribution (b) for the Herten aquifer analog .

arithmetic mean values taken from the aquifer analog data set (hydraulic conductivity: 2.1×10^{-3} m s^{-1}; specific storage: 6.6×10^{-5} m^{-1}).

Five wells are positioned in the center of the model domain. The wells are arranged in a five point star configuration, with the four outer wells located at a distance of 2.5 m from the center well (Figs. 2a and b). The initial head and the constant head at the boundaries are set to 0.2 m above the aquifer top, and confined conditions are confirmed during the simulation of pumping tests. For each pumping test, the simulation length is 300 s and six stress

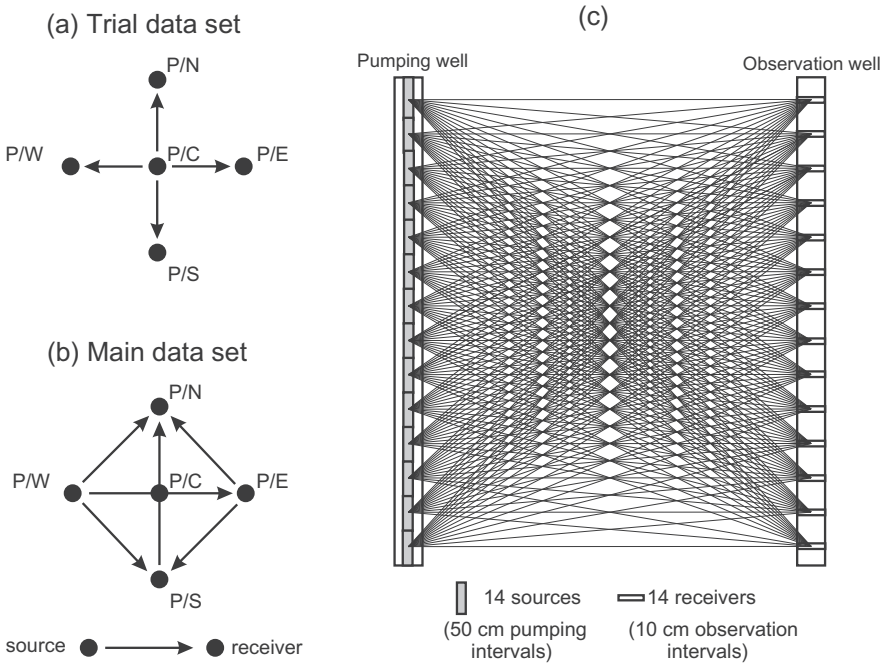

Fig. 2. Spatial position of pumping and observation wells of (a) trial data set for preliminary testing and (b) main data set. (c) Vertical position of the pumping and observation intervals of a recorded tomographic profile.

periods with 100 time steps in total are applied to simulate the drawdown phase.

Fifty-six pumping tests are simulated in this work. The pumping well is separated in 14 intervals with lengths of 0.5 m. During a simulated short term pumping test, the water is pumped out of one interval (each pumping interval consists of 5 cells in the vertical direction and each cell is defined as a pumping cell with 1/5 of the total pumping rate) and the pressure changes are recorded in the respective observation wells at all 14 different depths (each observation interval consists of one single cell with 10 cm cell thickness) that are arranged regularly over the whole thickness of the aquifer. The distance between adjacent observation points is 0.5 m. In successive tests, the pumping interval is changed to the adjacent interval, so that 14 tests are performed in total within one pumping well. Each pair of pumping-observation wells delivers 14×14 recorded transient pressure responses, which together form a cross-well vertical cross section of data (termed profile in the following) between the two wells. Fig. 2c displays the spatial position of the test and observation intervals along the test well and observation well, respectively, and the simulated test-observation configuration between the two wells is also presented.

For this work, a trial data set is first generated for fast preliminary testing. The trial data set includes four profiles, where the center well of the five point star configuration serves as source and the four surrounding wells are the observation wells (Fig. 2a). Using the trial data set and two-dimensional (2-D) travel time inversions, a strategy based on (i) the inversion of data subsets and (ii) the inversion of early travel times is developed.

In the subsequent main simulation, the chosen cross-well configurations allowed for the generation of a complete 3-D main data set. This covers six profiles recorded between each of all possible pairs of the four outer wells (Fig. 2b). This means that the center well of the five star configuration is not used.

Different from the first trial data set, this main data set is a complete data set, which covers not only the profiles of the NS and WE directions, but also the four sides of the five-well area. From the recorded pressure responses, the derived travel times are inverted via a 3-D inversion, applying the developed inversion strategy.

3. Inversion

The proposed inversion scheme couples two different techniques, which are travel time and steady shape inversions. The goal is to reconstruct the two parameters, hydraulic conductivity and specific storage, with high accuracy in two and three dimensions. Hydraulic travel times are governed by the hydraulic diffusivity, the ratio of hydraulic conductivity to specific storage, whereas the steady-shape drawdown configuration is determined solely by hydraulic conductivity. Thus, combining these two approaches will allow the identification of the two parameters hydraulic conductivity, diffusivity and consequently their ratio, i.e. specific storage. The entire inversion procedure is shown in Fig. 3.

The 2-D trial data set is intended to be utilized for fast preliminary testing, in order to optimize the travel time inversion strategy for the 3-D main data set. Testing the travel time inversion based on specific data subsets is done with the goal to increase the vertical resolution of the reconstructions. The procedure will be introduced in detail later in this section. In this context, the propagation of a pressure pulse is a fully three-dimensional diffusion phenomenon and the inversion of a three-dimensional pressure pulse, using a two dimensional parameter space, is an approximation of the real situation. Hence, the 2-D trial data set is a compromise between the possibility of fast preliminary testing and reliability.

From the full 3-D travel time inversion, both the spatial diffusivity pattern and the zonation of hydraulic conductivity are derived. A priori assumptions about the spatial distribution of hydraulic properties are desirable in order to incorporate (soft) geological knowledge and to mitigate the ill-posedness of the inverse problem. For example, sedimentary aquifers such as the inspected one are typically built up by potentially heterogeneous facies patterns rather than showing continuous property variations. Depending on the spatial wavelength of the propagation of the pressure pulse, reconstructed parameter distributions might be characterized by smearing effects and ambiguity. In order to overcome this we exploit the results of the travel time inversion to interpret the natural zonation of the hydraulic parameters. By this the number

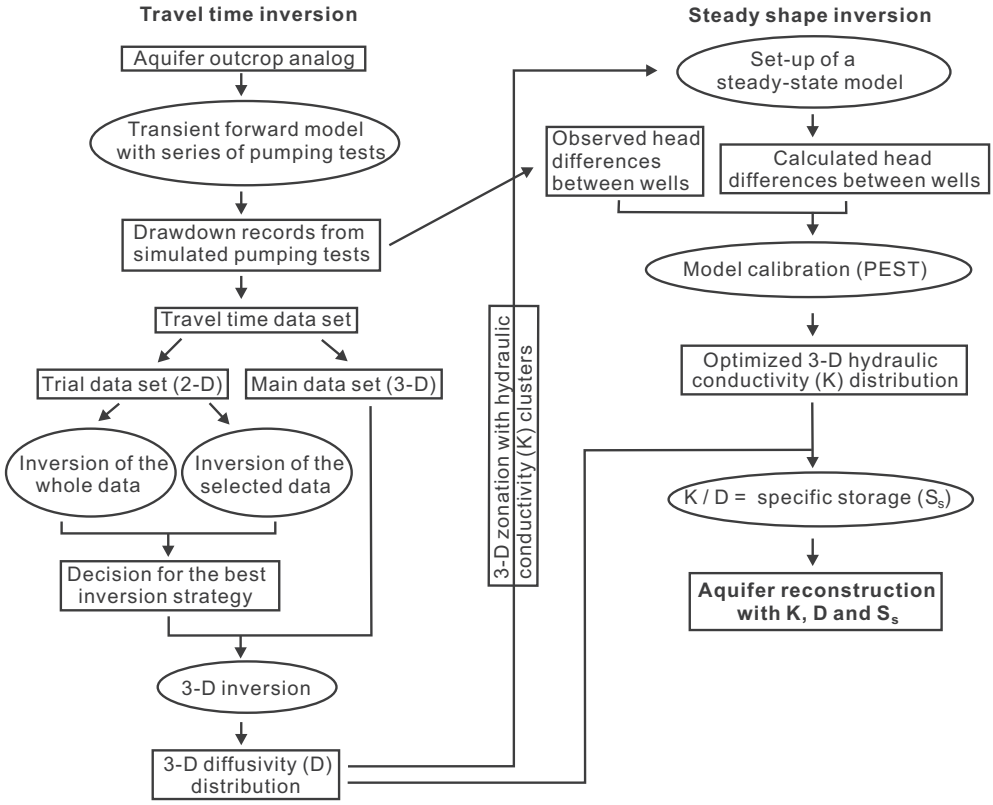

Fig. 3. Flowchart of the entire inversion procedure.

of unknowns of the steady shape inversion problem is minimized, while ensuring a geologically plausible reconstruction. The zonation is implemented in a steady-state model for the next step, the steady-shape inversion. This new flow model simulates the same configuration of pumping tests as examined with virtual reality, i.e. the original transient forward model. The model is then calibrated by adjusting the zoned hydraulic conductivities. This is done by minimization of head differences between the steady state zoned model and the transient original model. Based on the optimized hydraulic conductivity distribution from the steady-shape inversion and the diffusivity distribution from the hydraulic travel time inversion, the specific storage values can be calculated for the corresponding zonation and the aquifer can be fully reconstructed with these three parameters.

In the following, we describe the two inversion techniques and assess the potential of the combined inversion scheme for spatial reconstruction and identification of hydraulically significant subsurface features, e.g. potential preferential flow paths, and their properties.

3.1. Travel time based inversion

The key element of the proposed travel time based inversion approach is a line integral relating the arrival time of a hydraulic signal to the reciprocal value of diffusivity (Vasco et al., 2000; Kulkarni et al., 2000):

$$\sqrt{t_{\text{peak}}(x_2)} = \frac{1}{\sqrt{6}} \int_{x_1}^{x_2} \frac{ds}{D(s)} \tag{1}$$

where t_{peak} is the travel time of the peak of a Dirac signal from point x_1 (source) to observation point x_2 (receiver) along the arc-length (s) and D is the diffusivity.

The travel time integral (Eq. (1)) is only valid for an impulse source (Dirac pulse). However, Vasco et al. (2000) have shown that the pressure response of a Heaviside source can be transformed into a pressure response of an impulse source (Dirac source) by differentiation of the transient head data. This allows us to apply the inversion scheme to the pressure responses of constant rate pumping tests. For illustration, Fig. 4a shows a drawdown curve from a simulated pumping test; Fig. 4b depicts the slope of this drawdown (m s^{-1}), derived by differentiating, and the percentage (%) of the maximum amplitude at peak time.

In this work the travel time inversion approach is focused on the inversion of an early travel time (in the following called travel time diagnostic). A travel time diagnostic is defined as the time of occurrence of a certain feature of the transient pressure pulse. For example, the $t-10\%$ diagnostic is the time at which the pressure pulse rises to 10% of its ultimate peak value (Fig. 4b). In this sense, the peak value is defined as the $t-100\%$ diagnostic.

For the inversion of additional travel time diagnostics besides the peak time, a transformation factor was introduced by Brauchler et al. (2003):

$$\sqrt{t_{\alpha,d}} = \frac{1}{\sqrt{6 f_{\alpha,d}}} \int_{x_1}^{x_2} \frac{ds}{\sqrt{D(s)}} \tag{2}$$

where $t_{\alpha,d}$ is the respective travel time diagnostic and $f_{\alpha,d} = t_{peak}/t_{\alpha,d}$ is the related transformation factor. The subscript d denotes a Dirac source. The transformation factor is defined as follows:

$$f_{\alpha,d} = -W\left(-\frac{\alpha_d^{2/3}}{e}\right) \tag{3}$$

W denotes Lambert's *W function*. The head ratio α_d enables the comparison of the peak time with the respective travel time diagnostic: $h_d(r,t) = \alpha_d h_d(r, t_{\text{peak}})$, where $h_d(r,t)$ is the hydraulic head depending on space and time.

In order to test different inversion strategies, 2-D inversions based on the trial data set and the travel time diagnostic $t-10\%$

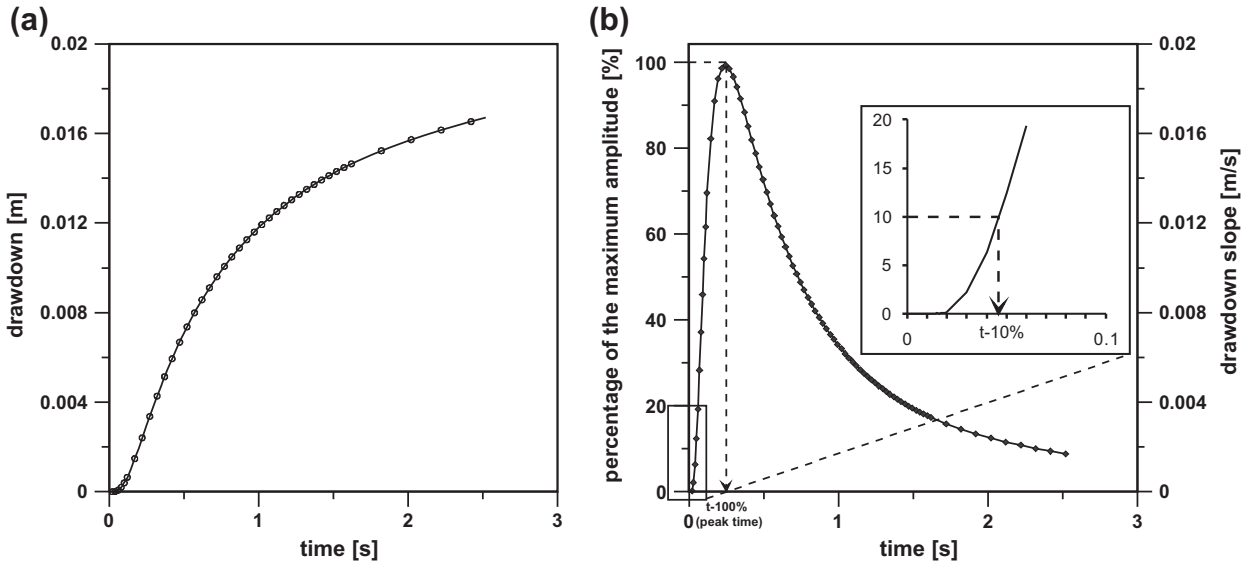

Fig. 4. (a) Drawdown curve from a simulated pumping test. (b) Slope of this drawdown ($m\ s^{-1}$) and percentage (%) of maximum amplitude at peak time.

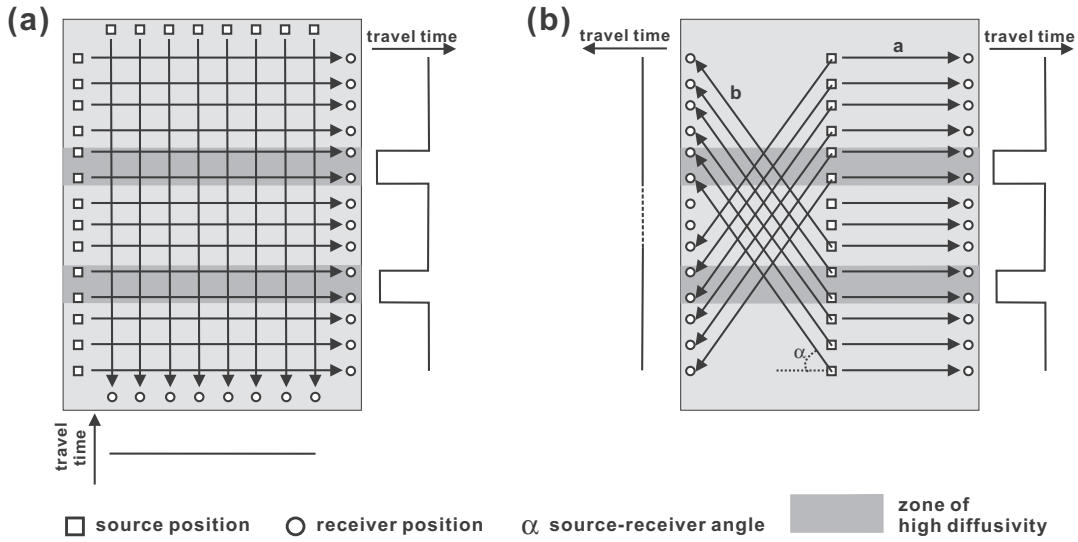

Fig. 5. Illustration of travel times based on data subsets with different source–receiver angles.

are carried out first. The inversion yields an estimated diffusivity distribution (in the following termed tomograms) for each profile between pumping and observation wells. The decision to use the travel time diagnostic $t - 10\%$ is based on the findings by Brauchler et al. (2007) and Cheng et al. (2009) that the tomograms based on the inversion of early travel time diagnostics show more details about subsurface heterogeneity. As described by Fermat's principle, the hydraulic signal prefers to follow the fastest path between source and receiver. Thus early travel times are more characteristic for the preferential flow paths. In contrast, later travel times, which characterize the final part of the signal, reflect the integral behavior throughout the whole area of investigation.

Another important point for the quality of subsurface transport predictions is the continuity and interconnectivity of the hydraulically significant subsurface features. To address this, we introduced the travel time inversion based on specific data subsets in addition to the inversion of a whole data set. This specific data subset refers to selected travel time series from the whole data set, which has a constraint on the angle between the horizontal and a straight line connecting the source and receiver (α). As shown in Fig. 5a, purely horizontal trajectories can only provide information regarding vertical variation because they average out horizontal variations, and similarly, purely vertical trajectories (if we could obtain them) would only provide information regarding horizontal variation. Hence, travel times of trajectories with larger source–receiver angles (e.g. trajectory "b" in Fig. 5b) indicate horizontal velocity changes (e.g. pinching out of a horizontal layer) and do not contribute much to the vertical resolution of the layered zones, compared with the trajectories "a". Under perfect conditions, the latter will improve the inversion. In practice, however, due to sparse data, spatially varying trajectory density and data inaccuracy, a potentially ill-posed inverse problem has to be solved (Tarantola, 2005). Under such conditions there is a risk that the gain from travel times with small information content is masked by the

non-uniqueness of the inversion solution. This can lead to smearing effects, ambiguity and undesirable artefacts (Becht et al., 2004; Brauchler et al., 2007).

The aquifer analog in our case, derived from a fluvial unconsolidated sedimentary outcrop, is dominated by features that show a larger extent in horizontal direction than in vertical direction. Hence we decided to compare different small-angle subsets of the trial data set for travel time inversion. The best inversion strategy with regard to a certain constraint on $|\alpha|$ will then be adopted for the full 3-D travel time inversion based on the main data set (Figs. 2b and 3).

The travel times for the diffusivity reconstructions are inverted using the software GeoTom3D, which is based on the Bureau of Mines tomography program 3DTOM (Jackson and Tweeton, 1996). The program was originally developed for seismic ray tomography and is based on the SIRT (Simultaneous Iterative Reconstruction Technique) algorithm (Gilbert, 1972) to determine the seismic velocities by integration of travel times:

$$t = \int_{x_1}^{x_2} \frac{ds}{v(s)} \tag{4}$$

The similarity between the seismic and hydraulic travel time inversions (Eq. (2) and (4)) allows us to use the same application software GeoTom3D to solve hydraulic tomographic problems. In our case, a model of GeoTom3D will be created with a homogeneous starting value for the diffusivity field, which is derived from the mean values of the measured source–receiver-combinations. The SIRT and ray bending algorithms are then employed to choose a diffusivity distribution which minimizes the function J:

$$J = \sum_{i=1}^{n} \left(\sqrt{t_i^m} - \sqrt{t_i^e} \right)^2, \tag{5}$$

where t_i^e and t_i^m are the estimated and measured travel times for the ith measurement, respectively, and n is the number of measurements. A detailed derivation of the SIRT algorithm with regard to the inversion of transient pressure responses is given in Appendix A.

Eqs. (2) and (4) are converted to a discrete problem by approximating the line integrals with a summation. The summation comprises one equation for each cell or unknown, respectively. Therefore, the number of cells should be adapted to the number of simulated source–receiver configurations in order to come close to an "even-determined problem". In even-determined problems there is just sufficient information to uniquely determine the model parameters (Menke, 1989). Furthermore the spatial variability of the trajectory density has to be taken into account. For cross-well experiments the trajectory density at the top and the bottom is always smaller than in the center of the model domain. Hence, in the tomograms presented in the following the number of cells is always chosen slightly smaller than the number of available source–receiver configurations.

3.2. Steady shape inversion

The key point of this study is to combine hydraulic travel time inversion and the steady shape analysis to separate the D value into its components K and S_s. Under steady shape conditions, drawdown varies with time but the hydraulic gradient does not. This means the head difference between two observation points does not vary and is characteristic for the K value, prior to the time when boundary conditions exert significant influence on the head response. Thus, we use a steady state model to analyze the transient data to increase the computational efficiency. Since the specific storage does not have any influence on the head difference, K is the only parameter to be determined. According to Butler (1988) and Cooper and Jacob (1946), for a homogeneous confined aquifer, the time required to reach steady shape conditions for constant-rate pumping tests with fully penetrating wells is given by $t > 100\, r^2\, S\, 4^{-1}\, T^{-1}$, where r is the distance from the pumping well (in our case 2.5 m and 5 m), S is storativity (4.62×10^{-4}), and T is transmissivity (1.47×10^{-2} m^2 s^{-1}). With the effects of partial penetration and heterogeneity, the time for the establishment of a steady shape condition is expected to be not more than 30 s in our case. Besides that, the response data derived from the transient model have shown that the steady shape condition has already been established at approximately 50 s after pumping. For the steady shape model, we take observed head difference values from the forward transient model, which are recorded at the 300th second.

The steady shape inversion is performed with a steady state flow model set-up using MODFLOW-96 (Harbaugh and McDonald, 1996). The zonation of the hydraulic conductivity field of the steady sate model is derived from the diffusivity field, which is reconstructed by travel time inversion (Fig. 3). The steady shape model

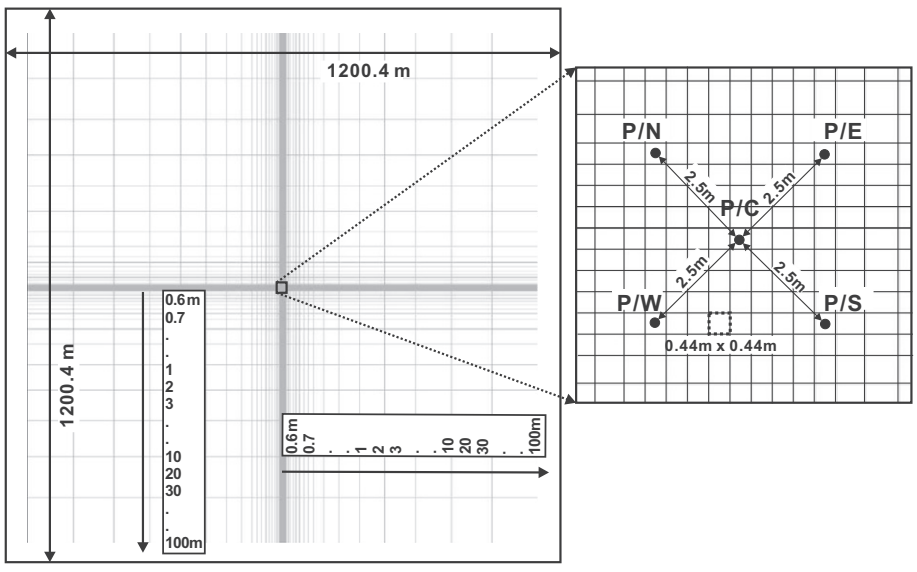

Fig. 6. Model domain used for the steady shape inversion with zoomed section of central well positions.

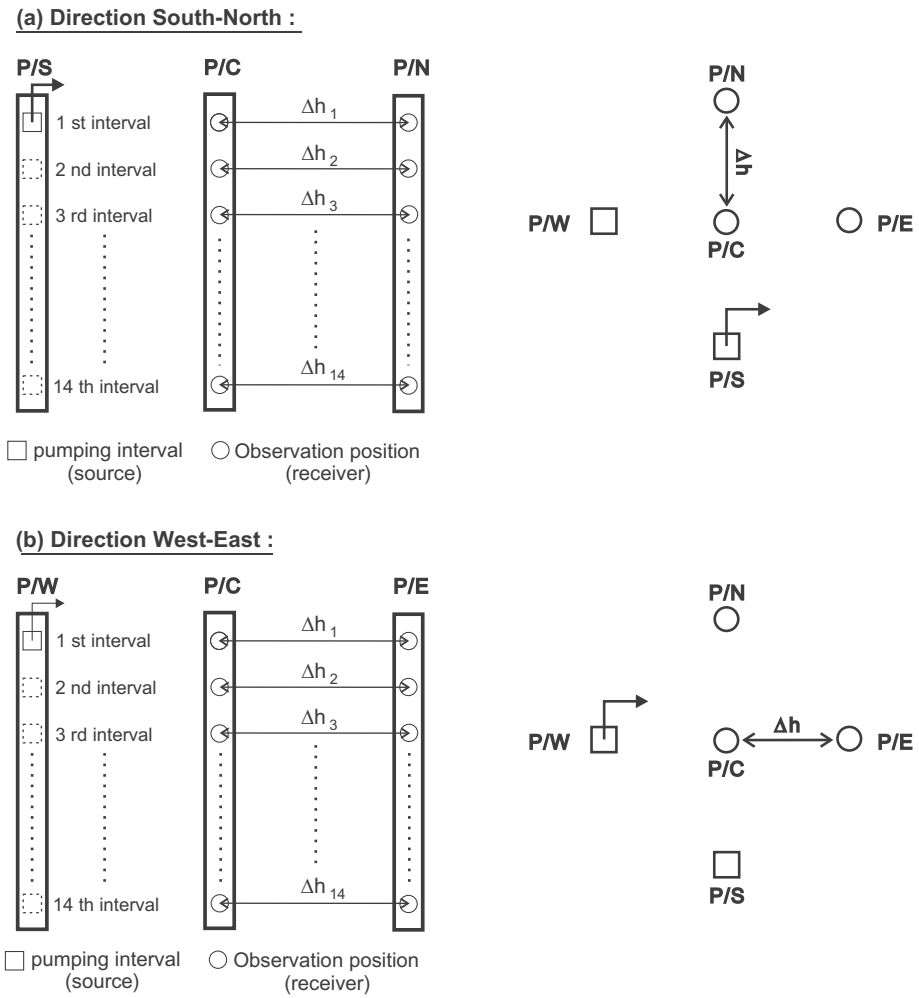

Fig. 7. Head differences recorded in two directions for the steady shape inversion: (a) South–North direction with pumping well P/S. (b) West–East direction with pumping well P/W.

domain can be separated into two parts. The center part reflecting the five point star configuration with a diagonal length of 5 m and an aquifer height of 7 m is discretized by voxels with an edge length of 0.44 m × 0.44 m × 0.44 m. Thereby, the cell length of the steady shape model is adapted to the voxel length of the three-dimensional diffusivity reconstruction.

Outside this area the model is extended by about 600 m in order to avoid any boundary effects. The model edges are represented by constant head boundaries (Fig. 6).

Using this model, pumping tests with the same configurations as in the full model based on analog data are simulated. The calculated steady shape head differences between two observation points are recorded and compared with those "observed" with the "true" analog data model. Note that for the steady shape inversion head differences rather than absolute head values are used (Bohling et al., 2002). Applying the automatic parameter estimator PEST (Doherty, 2003), the hydraulic conductivity field is found that minimizes the error between all calculated and observed head differences. As standard error measurement the root mean squared error (RMSE) is taken. Since the value of the RMSE is case-specific, we introduce the correlation coefficient as another general measure of goodness of fit.

For the parameter estimation, 392 ($14 \times 14 + 14 \times 14$) recorded head differences from a series of 28 short term pumping tests are used. The recorded head differences can be divided into two directions (Fig. 7). Direction South-North is based on 14 pumping tests with the pumping well P/S. Consistent with the tomograms of the full data set, the pumping well is screened every 0.5 m during each pumping test. The head differences generated by each pumping test are recorded at 14 different depths between the center well P/C and well P/N. Direction West–East is recorded using the same set-up between the pumping well P/W and the observation wells P/E and P/C. Note that there are 43,120 possible head difference pairs from the 56 simulated pumping tests. For computational efficiency, we did not include all of the possible data pairs. As introduced in Bohling et al. (2002), different or more sets of data pairs make little significant difference in the estimation results, if an already large number of data pairs are selected.

4. Results

4.1. Travel time based inversion results

The trial data set includes four profiles that form a cross with the central well P/C serving as the pumping well (Fig. 2a). Travel time based inversion is applied to arrive at four independently inverted profiles. In West–East (WE) and South–North (SN) direction, the two adjacent profiles each are combined and two composite tomograms are derived. Tomogram WE represents the reconstructed aquifer between the wells P/C – P/W and P/C – P/E. Profile

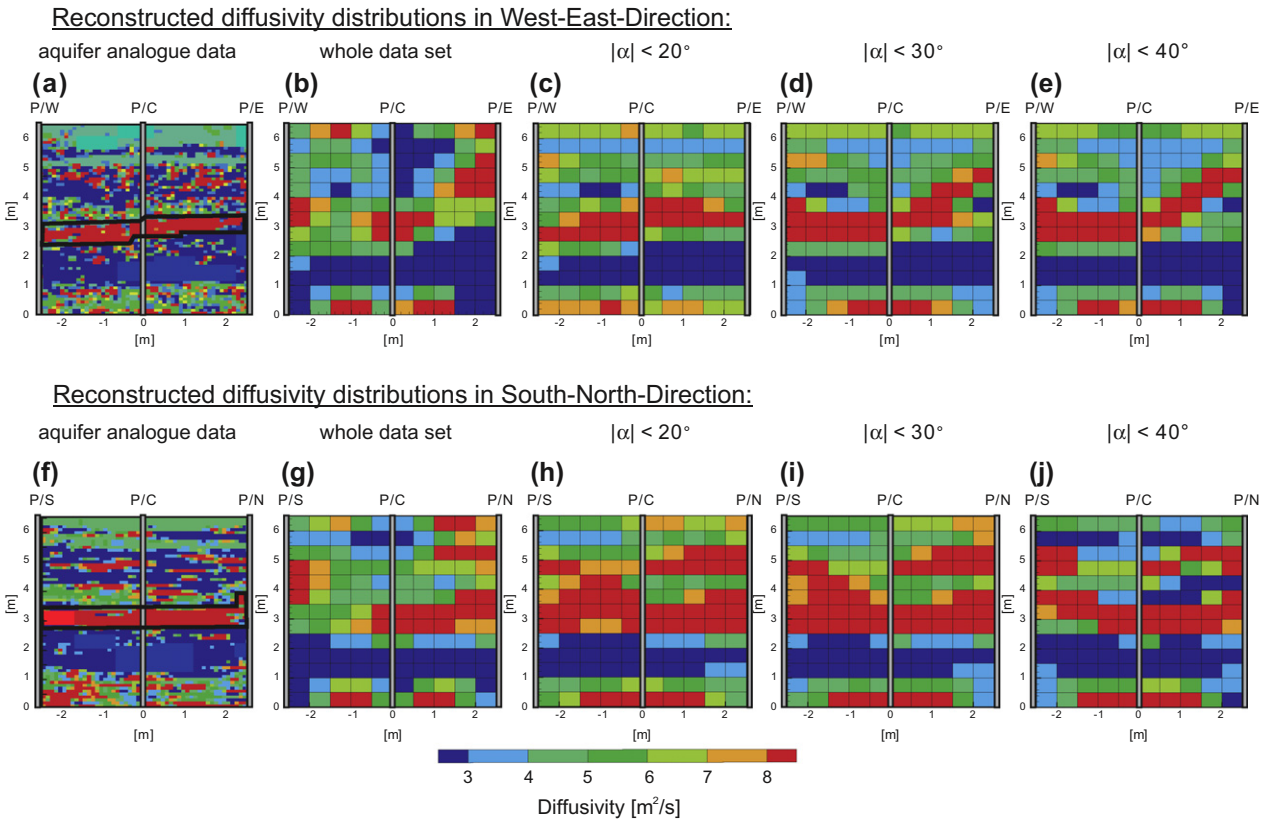

Fig. 8. Comparison of the aquifer analog data with the reconstructed diffusivity values: (a–e) Profiles in West–East direction. (f–j) Profiles in South–North direction.

SN is oriented perpendicularly and based on the profiles between the wells P/C – P/S and P/C – P/N (Fig. 2a).

Fig. 8b and g display the obtained composite diffusivity tomograms, using the whole data set of travel times. Comparison with the "true" high resolution aquifer analog data (Fig. 8a and f) reveals that significant hydraulic features of the aquifer could be reconstructed. The comparatively coarse resolution of the tomograms does not allow for the reconstruction of those zones with small scale variability in hydraulic parameters. However, they capture in particular the extensive and continuous portions such as the horizontal low-diffusivity zone in the lower half of the analog. Even the high diffusivity zone in the center of both analog sections (bold black lines in Fig. 8a and f) is detected, especially in the SN-tomogram. However the reconstruction of the laterally continuous high diffusivity zones in the middle of the aquifer, as well as of the low-diffusivity zone close to the aquifer top, is still not satisfactory. In order to improve the interpretation, travel time inversion based on specific data subsets in addition to the whole trial data set is suggested. As shown in Fig. 8, the inversion results based on the trajectories with $|\alpha| < 20°$, $|\alpha| < 30°$ and $|\alpha| < 40°$ also reflect the main hydraulically significant features. Additionally, all these reconstructions indicate that the high permeability zone in the center of the SN as well as of the WE section is continuous. These results are in agreement with the findings of Brauchler et al. (2007), which demonstrated for a synthetic case that the resolution of horizontally arranged layers can strongly be improved using data subsets with small source–receiver angles. However, in our case there is a risk that better characterization of horizontal features would occur at the expense of reconstructing vertical or inclined structures, since at some depths the aquifer analog is also highly heterogeneous in the horizontal direction. As a compromise, the constraint on the source–receiver angle should not be too strict, and $|\alpha| < 40°$ is chosen for the subsequent full 3-D inversion of the main data set.

The 3-D inversion with the data subset of $|\alpha| < 40°$ from the main dataset yields tomograms of a resolution of $8 \times 8 \times 14$ voxels. For this application, the procedure takes 10 s on a 3.3 GHz Pentium CPU. Comparison of the reconstructed diffusivity field (Fig. 9b) with the "true" field (Fig. 9a) shows that, at this resolution, significant hydraulic features can be reconstructed with adequate precision. The 3-D reconstruction appears to be of higher quality than the 2-D results illustrated in Fig. 8. An apparent reason for these differences is that the simulated pressure pulses in fact propagate in three dimensions. The 2-D inversion of the pressure responses can hardly reflect 3-D processes and thus it is more an approximation and can lead to ambiguous results.

4.2. Steady shape inversion results

For the flow model of the following steady shape inversion, the zonation of equal hydraulic conductivity (Fig. 9c) is defined based on the results of the 3-D hydraulic travel time inversion (Fig. 9b). A principal advantage of the introduced zonation is its ability to overcome the shortcoming of the travel time based inversion approach to reconstruct discrete changes in hydraulic properties. The aquifer analog data set, for example, features open framework gravel layers with a K value of approximately 10^{-2} m s^{-1} (some even of 1 m s^{-1}) deposited next to sand-gravel mixtures with a K value of 5×10^{-5} m s^{-1}. Fig. 9 (mainly at depths of 3–4 m) shows that travel time based inversion fails to reconstruct such discrete changes but reconstructs smoothed interfaces with continuously changing parameter distributions.

Three clusters of constant diffusivity values are distinguished. Note that in this study the clusters denote diffusivity classes (i.e.

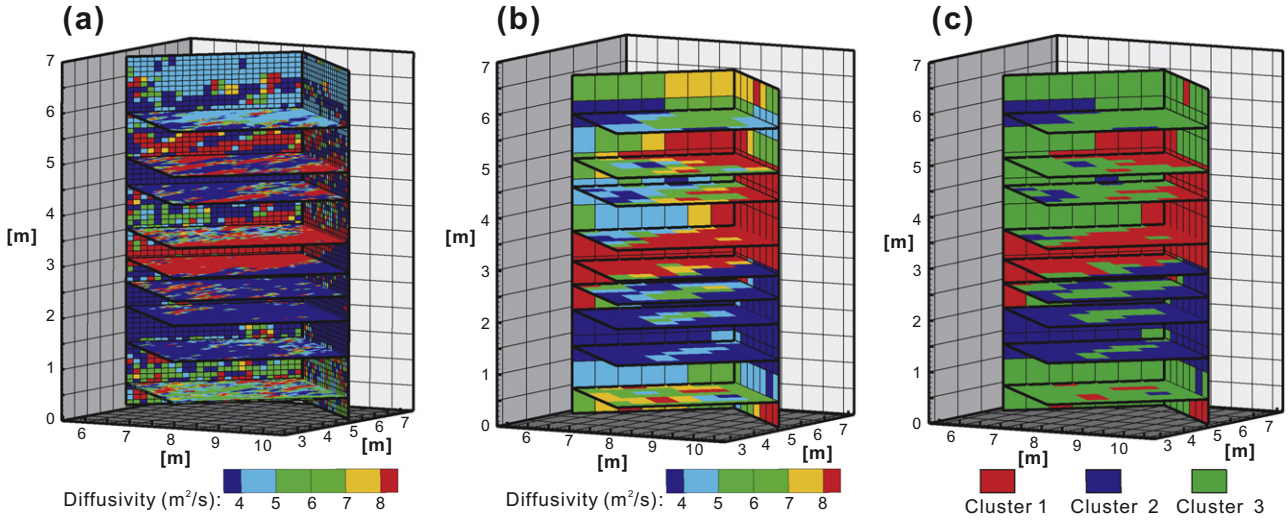

Fig. 9. (a and b) Comparison of the aquifer analog data with the three-dimensional diffusivity reconstruction. (c) Hydraulic zonation based on the results of the three dimensional hydraulic travel time inversion.

"facies"), whereas zones represent volume elements of the same diffusivity class. Due to the small number of clusters the derived model in Fig. 9c consists of three zones, which are fewer than those of the high-resolution original. Though they are non-uniform, of different size, and thus replicate the complex composition of the investigated medium, sediments with identical hydraulic properties (i.e. of the same hydrofacies) are deposited at different positions of the aquifer and are separated from each other.

The small number of clusters is chosen in accordance with the achievable resolution by the diffusivity tomogram, and it facilitates computationally efficient steady shape inversion. The clusters here are characterized as follows:

- Cluster 1 represents the highest permeable zones in the center of the diffusivity tomogram, located between 3 m and 3.5 m as well as 4.5 m and 5 m above aquifer analog bottom. This domain is characterized mainly by matrix free gravel, which is indicated by diffusivity values larger than 8 $m^2\,s^{-1}$.
- Cluster 2 covers the lowest permeable area located between 1 m and 3 m above the bottom directly below the high permeability zone represented by Cluster 1. A smaller section is located close to the top of the aquifer between 5.5 m and 6 m above bottom. Gravel sand mixtures dominate this cluster, leading to diffusivity values less than 4 $m^2\,s^{-1}$.
- The domain close to the top and bottom of the aquifer analog is represented by Cluster 3, which denotes intermediate diffusivity values. In the aquifer analog, this area is mainly characterized as sand-rich/stone-rich gravel, which is reflected by diffusivity values between 4 $m^2\,s^{-1}$ and 8 $m^2\,s^{-1}$.

The threshold values are chosen in a way that each hydraulically significant feature is assigned to a different cluster. The thresholding could be optimized by incorporating the zonation within the steady shape inversion scheme as described in Cardiff and Kitanidis (2009). However this would increase the computational burden and hence the big advantage of the combination of two calculation efficient inversion schemes could be masked.

Outside of the center part of the model a constant K value of $2 \times 10^{-3}\,m\,s^{-1}$ for the surrounding aquifer is assigned. Table 2 summarizes the starting values and the upper and lower bounds used for the steady shape inversion, which is performed using a steady state model with parameter estimator. This model has a zonation of K derived from the D-distribution. In each model run, the parameter estimator optimizes the K values by fitting the calculated head differences to the "observed head differences" obtained from the transient model. The parameter estimation procedure required 127 model runs on a PC with a 3.33 GHz CPU, and each run of the steady state model took about 25 s. The minimized root mean square error (RMSE) from the calculated and observed head differences amounts to 0.4 mm and the mean value of the 392 residuals between calculated and observed head differences is 4 mm.

The correlation coefficient R of observed and simulated head differences for the calibrated model is 0.8, which is considered acceptable keeping in mind the coarse resolution considered for the tomograms. Table 3 lists the estimated K values as well as the respective specific storage values for the three clusters. The specific storage values are calculated as the quotient of hydraulic conductivity over diffusivity. Additionally the arithmetic and harmonic means for the zones of the aquifer analog are given. These means represent the upper and lower bound of the equivalent conductivity of an up-scaled heterogeneous block, respectively (see e.g. Cardwell and Parsons, 1945). The comparison between the K values derived from the steady shape inversion with the mean true value ranges show a good agreement for all of the three clusters. The estimated values tend to be closer to the arithmetic mean. This reflects the mostly horizontal orientation of the sedimentary structures, at a small angle to the direction of the inspected trajectories. The diffusivity and derived specific storage values also lie in or close to the expected value ranges except for Cluster 1, which represents the high-D zone. Apparently, the travel time inversion approach is not able to reconstruct the full range of diffusivity within Cluster 1. Fig. 10 shows a histogram of the diffusivity distribution of this cluster. The diffusivity values range from 10^{-1} to $3 \times 10^4\,m^2\,s^{-1}$ with an arithmetic mean of 773 $m^2\,s^{-1}$, whereby the reconstructed diffusivity values range from 8 to 200 $m^2\,s^{-1}$ with an arithmetic mean of 20 $m^2\,s^{-1}$. The reason for these

Table 2
Initial parameters and value bounds used for the steady shape inversion.

Cluster No.	Diffusivity ($m^2\,s^{-1}$)	Hydraulic conductivity ($m\,s^{-1}$)		
		Starting value	Lower bound	Upper bound
1	>8	1.0×10^{-4}	1.0×10^{-7}	1
2	<4	1.0×10^{-4}	1.0×10^{-7}	1
3	4~8	1.0×10^{-4}	1.0×10^{-7}	1

Table 3
Arithmetic means (arithm.) and harmonic means (harm.) as "true" values of hydraulic conductivity, specific storage and diffusivity for the three clusters and the corresponding estimated (est.) values.

Cluster No.	Hydraulic conductivity ($m\ s^{-1}$)			Diffusivity ($m^2\ s^{-1}$)			Specific storage (m^{-1})		
	Arithm.	Harm.	Est.	Arithm.	Harm.	Est.	Arithm.	Harm.	Est.
1	3.0×10^{-2}	1.5×10^{-5}	1.7×10^{-2}	773	0.2	20	7.7×10^{-5}	9.2×10^{-5}	8.5×10^{-4}
2	1.3×10^{-4}	8.9×10^{-5}	1.6×10^{-4}	1.6	1.0	2.1	9.4×10^{-5}	9.0×10^{-5}	7.6×10^{-5}
3	3.4×10^{-4}	2.7×10^{-4}	4.0×10^{-4}	6.6	5.0	5.8	5.4×10^{-5}	5.3×10^{-5}	6.9×10^{-5}

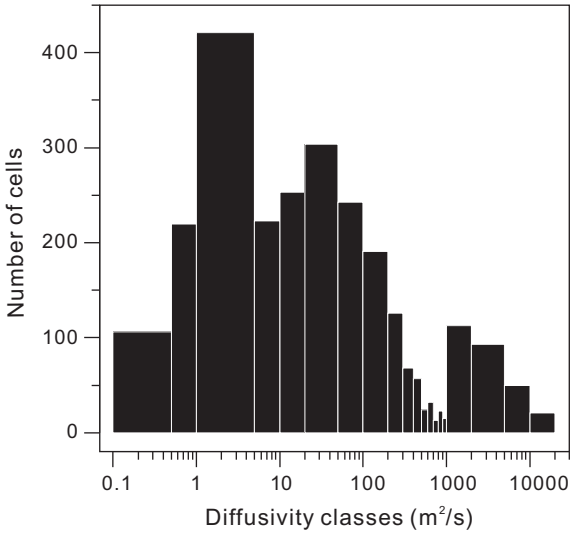

Fig. 10. Histogram of the diffusivity distribution of Cluster 1 representing the high-diffusivity zone in the center of the aquifer analog data set.

differences is the strong heterogeneous composition of the outcrop analog data. The stone rich gravel (matrix free hydrofacies cGcg,o in Table 1) characterized by diffusivity values between 2×10^4 and $3 \times 10^4\ m^2\ s^{-1}$ is not arranged in a horizontal layer but is distributed in small clusters. Numerical and experimental studies performed by Vasco et al. (2000) and Brauchler et al. (2007) have shown that parameter variations of several orders of magnitude can be reconstructed. However, for the transformation of the diffusivity equation into the eikonal equation, a hydraulic parameter distribution is assumed, which varies smoothly with respect to the spatial wavelength of the propagation of the pressure pulse. Therefore, the small clusters of stone rich gravel characterized by extremely high diffusivity values cannot be reconstructed. Nevertheless, the good agreement between the reconstructed and true hydraulic conductivity values, representing the most significant hydraulic properties, shows the potential of the combined inversion approach to characterize hydraulic properties of the subsurface with high resolution.

5. Conclusions

The potential of a combined hydraulic tomographic inversion approach is investigated with an aquifer analog outcrop model. The aquifer analog outcrop model allows one to appraise the potential of the combined tomographic inversion approach by numerical methods taking into account realistic aquifer heterogeneity. The proposed combined hydraulic tomographic inversion approach consists of two complementary and fast inversion techniques: hydraulic travel time and steady shape inversions.

We utilized the hydraulic travel time based tomography approach to determine clusters of the analog of constant diffusivity, and the steady shape inversion allowed the reconstruction of an average hydraulic conductivity estimate for each cluster. Finally a specific storage estimate could be calculated for each cluster based on the diffusivity and hydraulic conductivity estimates for each cluster.

The comparison with the aquifer analog data shows that the combined inversion approach allows reliable estimation of hydraulic conductivity. The travel time inversion, however, does not resolve the diffusivity distribution of one cluster that represents a highly heterogeneous part of the analog. Hence the interpreted specific storage for this cluster is too high. The underestimation of diffusivity, as well as the overestimation of the specific storage is due to the test design of hydraulic travel time tomography in our synthetic case study, which prevented us from resolving small scale variability of hydraulic conductivity with high discrepancies. Moreover, the hydraulic travel time based inversion is based on the transformation of the transient groundwater flow equation into the eikonal equation using an asymptotic approach. The transformation is only valid for media that vary smoothly with respect to the spatial wavelength of the propagation of the pressure pulse. Beyond this, the voxel size has to be adapted to the number of available measurements in order to avoid an ill posed inverse problem. Therefore, the small clusters of stone rich gravel characterized by high diffusivity values cannot be reconstructed.

Nevertheless it is possible to reconstruct the most significant hydraulic features by the travel time based inversion approach. A better reconstruction of the aquifer hydraulic parameters is expected by utilizing a larger amount of measurements, which involve more test and observation intervals. The zonation approach can serve as a starting model for further inversion techniques, next to the proposed inversion steady shape inversion. A promising approach in unconsolidated sediments is e.g. the coupling with high resolution direct-push profiling (Butler et al., 2007; Dietrich et al., 2008; Liu et al., 2009). Coupling this approach will help overcome the problems of non-uniqueness and uncertainty caused by the limitations of hydraulic tomography.

Acknowledgments

The investigations were conducted with the financial support of the German Research Foundation within the project "High resolution aquifer characterization based on direct-push technology: An integrated approach coupling hydraulic and seismic tomography" (Grant No. BR3379/1-2). This manuscript greatly benefited from comments by Geoffrey C. Bohling, Walter Illman and one anonymous reviewer.

Appendix A. SIRT algorithm

The description of the SIRT algorithm with regard to the inversion of transient pressure responses, given below, is partly based on the derivation given in Brauchler et al., 2007.

The 3-dimensional propagation of a Dirac source pressure pulse in the subsurface can be described by a line integral relating the arrival time of a "hydraulic signal" to the reciprocal value of diffusivity (Vasco et al., 2000; Kulkarni et al., 2000),

$$\sqrt{t_{\alpha,d}} = \frac{1}{\sqrt{6f_{\alpha,d}}} \int_{x_1}^{x_2} \frac{ds}{\sqrt{D(s)}} \tag{A1}$$

where D is the diffusivity as a function of arc-length along the propagation path (s). $t_{\alpha,d}$ is the respective travel time diagnostic and $f_{\alpha,d} = t_{peak}/t_{\alpha,d}$ is the related transformation factor, where t_{peak} is the travel time of the peak of a signal from the point x_1 (source) to the observation point x_2 (receiver).

The defined integral (A1) can be converted to a discrete inverse problem by approximating the integral with a summation

$$\sqrt{6f_{\alpha,d}t_i} = \sum_{j=1}^{n} \sqrt{\frac{1}{D_j}} d_{ij} \tag{A2}$$

where d_{ij} is the distance along trajectory i in cell j and D_j is the average diffusivity within cell j. In order to solve Eq. (A2) we have applied an iterative technique, where one equation (one trajectory) is analyzed at a time. The algorithm requires an initial diffusivity guess which can be easily determined by a conventional pumping test. An estimate for $\sqrt{6f_{\alpha,d}t_i}$ is calculated along each trajectory,

$$\sqrt{6f_{\alpha,d}t_i} = \sum_{j=1}^{n} \sqrt{\frac{1}{D_j^q}} d_{ij} \tag{A3}$$

where D_j^q indicates the estimated diffusivity after the qth iteration. Note that a single iteration includes an analysis of all trajectories. The goal of the inversion is to choose a diffusivity distribution which minimizes for each measured configuration the least squares discrepancy between the predicted and the measured travel times,

$$\Delta t_i = \left[\sqrt{6f_{\alpha,d}t_i^m} - \sqrt{6f_{\alpha,d}t_i^e}\right] = \sum_{j=1}^{n} \left(\Delta\sqrt{\frac{1}{D_j^q}} d_{ij}\right) \tag{A4}$$

with t_i^m the measured travel time, t_i^e the estimated travel time, Δt_i the difference of the ith measured and estimated travel time and $\Delta\sqrt{\frac{1}{D_j^q}}$ the necessary incremental correction for the qth iteration of cell j. Following Dines and Lytle (1979) an additional minimum criterion can be defined for the determination of the distribution of $\sqrt{\frac{1}{D_j^q}}$:

$$f\left(\Delta\sqrt{\frac{1}{D_j^q}}\right) = \sum_{j=1}^{n} \left(\Delta\sqrt{\frac{1}{D_j^q}}\right)^2 \rightarrow \min. \tag{A5}$$

The above equation corresponds to a minimum energy correction. Minimizing the function f subject to Eq. (A4) yields an update of the square root of diffusivity for each cell sampled by that trajectory i. The minimization can be performed by using the Lagrange multipliers method. Thereby we attempt to minimize the new function:

$$K = \sum_{j=1}^{n} \left[\left(\Delta\sqrt{\frac{1}{D_j^q}}\right)^2 - \lambda\Delta\frac{1}{D_j^q} d_{ij}\right] + \lambda\Delta t_i \tag{A6}$$

Zeroing the first derivative of the above equation, we get:

$$\Delta\sqrt{\frac{1}{D_j^q}} = \frac{\lambda d_{ij}}{2} \tag{A7}$$

and substituting into Eq. (A4) we get for λ:

$$\lambda = \frac{2\Delta t_i}{\sum_{j=1}^{n} d_{ij}^2} \tag{A8}$$

We receive the final solution by substituting Eq. (A8) into (A7). Thus, the minimization leads for a particular trajectory i, in the qth iteration to the incremental correction:

$$\Delta\sqrt{\frac{1}{D_{ij}^q}} = \frac{\Delta t_i d_{ij}}{\sum_{j=1}^{n} d_{ij}^2} \tag{A9}$$

After all N trajectories have been analyzed, the corrections are applied by averaging the incremental corrections of each single cell

$$\Delta\sqrt{\frac{1}{D_j^q}} = \frac{1}{M_j} \sum_{i=1}^{N} \Delta\sqrt{\frac{1}{D_{ij}^q}} \tag{A10}$$

where M_j is the number of trajectories passing through cell j.

References

Bayer, P., 1999. Aquifer-Analog-Studie in grobklastischen braided river Ablagerungen: Sedimentäre/hydrogeologische Wandkartierung und Kalibrierung von Georadarmessungen, Diplomkartierung. Universität Tübingen.

Bayer, P., Huggenberger, P., Renard, P., Comunian, A., 2011. Three-dimensional high resolution fluvio-glacial aquifer analog. Part 1: Field study. Journal of Hydrology. doi:10.1016/j.jhydrol.2011.03.038.

Becht, A., Tronicke, J., Appel, E., Dietrch, P., 2004. Inversion strategy in crosshole radar tomography using information of data subsets. Geophysics 69, 220–230.

Bohling, G.C., 2009. Sensitivity and resolution of tomographic pumping tests in an alluvial aquifer. Water Resour. Res. 45, W02420. doi:10.1029/2008WR007249.

Bohling, G.C., Butler Jr., J.J., 2010. Inherent limitations of hydraulic tomography. Ground Water. doi:10.1111/j.1745-6584.2010.00757.x.

Bohling, G.C., Zhan, X., Butler Jr., J.J., Zheng, L., 2002. Steady shape analysis of tomographic pumping tests for characterization of aquifer heterogeneities. Water Resour. Res (3812), 1324.

Bohling, G.C., Butler Jr., J.J., Zhan, X., Knoll, M.D., 2007. A field assessment of the value of steady shape hydraulic tomography for characterization of aquifer heterogeneities. Water Resour. Res. 43, W05430 (p. 21).

Brauchler, R., Liedl, R., Dietrich, P., 2003. A travel time based hydraulic tomographic approach. Water Resour. Res. 39 (12/1370), WR002262. doi:10.1029/2003.

Brauchler, R., Cheng, J., Everette, M., Johnson, B., Dietrich, P., Liedl, R., Sauter, M., 2007. An inversion strategy for hydraulic tomography: coupling travel time and amplitude inversion. J. Hydrol. 345, 184–198. doi:10.1016/j.jhydrol.2007.08.011.

Brauchler, R., Hu, R., Vogt, T., Halbouni, D., Heinrichs, T., Ptak, T., Sauter, M., 2010. Cross-well slug interference tests: an effective characterization method for resolving aquifer heterogeneity. J. Hydrol. 384, 33–45. doi:10.1016/j.jhydrol.2010.01.004.

Brauchler, R., Hu, R., Dietrich, P., Sauter, M., 2011. A field assessment of high-resolution aquifer characterization based on hydraulic travel time and hydraulic attenuation tomography. Water Resour. Res. 47, W03503. doi:10.1029/2010 WR009635.

Butler Jr., J.J., 1988. Pumping tests in nonuniform aquifers – the radially symmetric case. J. Hydrol. 101, 15–30.

Butler Jr., J.J., 2005. Hydrogeological methods for estimation of hydraulic conductivity. In: Rubin, Y., Hubbard, S.S. (Eds.), Hydrogeophysics. Springer, Dordrecht, The Netherlands, pp. 23–58.

Butler Jr., J.J., McElwee, C.D., Bohling, G.C., 1999. Pumping tests in networks of multilevel sampling wells: motivation and methodology. Water Resour. Res. 35 (11), 3553–3560.

Butler Jr., J.J., Dietrich, P., Wittig, V., Christy, T., 2007. Characterizing hydraulic conductivity with the direct-push permeameter. Ground Water 45 (4), 409–419.

Cardiff, M., Kitanidis, P.K., 2009. Bayesian inversion for facies detection: an extensible level set framework. Water Resour. Res. 45, W10416. doi:10.1029/2008WR007675.

Cardiff, M., Barrash, W., Kitanidis, P.K., Malama, B., Revil, A., Straface, S., Rizzo, E., 2009. A potential-based inversion of unconfined steady-state hydraulic tomography. Ground Water 47 (2), 259–270. doi:10.1111/j.1745-6584.2008.00541.x.

Cardwell Jr., W.T., Parsons, R.L., 1945. Average permeabilities of heterogeneous oil sands. Trans. Am. Inst. Min. Metall. Pet. Eng. 160, 34–42.

Cheng, J.T., Brauchler, R., Everett, M.E., 2009. Comparison of early and late travel times of pressure pulses induced by multilevel slug tests. Eng. Appl. Comput. Fluid Mech. 3 (4), 514–529.

Cooper Jr., H.H., Jacob, C.E., 1946. A generalized graphical method for evaluating formation constants and summarizing well field history. Trans. AGU 27, 526–534.

Datta-Gupta, A., Kulkarni, K.N., Yoon, S., Vasco, D.W., 2001. Streamlines ray tracing and production tomography: generalization to compressible flow. Petroleum Geosci. 7, 75–86.

Dietrich, P., Butler Jr., J.J., Faiß, K., 2008. A rapid method for hydraulic profiling in unconsolidated formations. Ground Water 46 (2), 323–328.

Dines, K.A., Lytle, R.J., 1979. Computerized geophysical tomography. Proc. IEEE 67, 1065–1073.

Doherty, J., 2003. Version 5 of PEST Manual. Watermark Numerical Computing, Brisbane, Australia.

Domenico, P.A., Mifflin, M.D., 1965. Water from low-permeability sediments and land subsidence. Water Resour. Res. 1 (4), 563–576. doi:10.1029/WR001i004p00563.

Farrell, D.A., Woodbury, A.D., Sudicky, E.A., 1994. The 1978 Borden tracer experiment: analysis of the spatial moments. Water Resour. Res. 30 (11), 3213–3223.

Fienen, M.N., Clemo, T., Kitanidis, P.K., 2008. An interactive Bayesian geostatistical inverse protocol for hydraulic tomography. Water Resour. Res. 44, W00B01. doi:10.1029/2007WR006730.

Flint, S.S., Bryant, I.D., 1993. The Geological Modelling of Hydrocarbon Reservoirs and Outcrop Analogues. Special Publication of the International Association of Sedimentologists, vol. 15. Blackwell Scientific Publications, Oxford.

Gilbert, P., 1972. Iterative methods for the three-dimensional reconstruction of an object from projections. J. Theor. Biol. 36 (1), 105–117. doi:10.1016/0022-5193(72)90180-4.

Gottlieb, J., Dietrich, P., 1995. Identification of the permeability distribution in soil by hydraulic tomography. Inverse Problems 11, 353–360.

Harbaugh, A.W., McDonald, M.G., 1996. User's Documentation for MOD- FLOW-96, An Update to the US Geological Survey Modular Finite-difference Ground-water Flow Model. US Geological Survey Open-File Report 96-485.

He, Z., Datta-Gupta, A., Vasco, D.W., 2006. Rapid inverse modeling of pressure interference tests using trajectory-based traveltime and amplitude sensitivities. Water Resour. Res. 42, W03419. doi:10.1029/2004WR003783.

Huggenberger, P., Aigner, T., 1999. Introduction to the special issue an aquifer-sedimentology: problems, perspectives and modern approaches. Sediment Geol. 129 (3–4), 179–186.

Illman, W.A., Craig, A.J., Liu, X., 2008. Practical issues in imaging hydraulic conductivity through hydraulic tomography. Ground Water 46 (1), 120–132.

Illman, W.A., Liu, X., Takeuchi, S., Yeh, T.-C.J., Ando, K., Saegusa, H., 2009. Hydraulic tomography in fractured granite: Mizunami Underground Research site, Japan. Water Resour. Res. 45, W01406. doi:10.1029/2007WR006715.

Illman, W.A., Zhu, J., Craig, A.J., Yin, D., 2010. Comparison of aquifer characterization approaches through steady state groundwater model validation: a controlled laboratory sandbox study. Water Resour. Res. 46, W04502. doi:10.1029/2009WR007745.

Jackson, M.J., Tweeton, D.R., 1996. 3DTOM: Three-Dimensional Geophysical Tomography. Report of Investigations 9617. US Department of the Interior, p. 84.

Jacob, C.E., 1963. Determining the permeability of water-table aquifers, in methods of determining permeability, transmissibility, and drawdown (compiled by R. Bentall). US Geol. Surv. Water Supply Pap. 1536-I, 245–271.

Kruseman, G.P., de Ridder, N.A., 1990. Analysis and Evaluation of Pumping Test Data. ILRI Publ. 47. Int. Inst. for Land Reclam. and Impr, Wageningen, Netherlands, 377 pp.

Kulkarni, K.N., Datta-Gupta, A., Vasco, D.W., 2000. A streamline approach to integrating transient pressure data into high resolution reservoir models. SPE J. 6 (3), 273–282.

Li, W., Englert, A., Cirpka, O., Vanderborght, J., Vereecken, H., 2007. Two-dimensional characterization of hydraulic heterogeneity by multiple pumping tests. Water Resour. Res. 43, W04433. doi:10.1029/2006WR005333.

Li, W., Englert, A., Cirpka, O., Vereecken, H., 2008. Three-dimensional geostatistical inversion of flowmeter and pumping test data. Ground Water 46 (2), 193–201.

Liu, S., Yeh, T.-C.J., Gardiner, R., 2002. Effectiveness of hydraulic tomography: sandbox experiments. Water Resour. Res. 38, 04. doi:10.1029/2001WR000338.

Liu, X., Illman, W.A., Craig, A.J., Zhu, J., Yeh, T.-C.J., 2007. Laboratory sandbox validation of transient hydraulic tomography. Water Resour. Res. 43, W05404–0000. doi:10.1029/2006WR005144.

Liu, G., Butler Jr., J.J., Bohling, G.C., Reboulet, E., Knobbe, S., Hyndman, D.W., 2009. A new method for high-resolution characterization of hydraulic conductivity. Water Resour. Res. 45, W08202. doi:10.1029/2009WR008319.

Maier, U., DeBiase, C., Baeder-Bederski, O., Bayer, P., 2009. Calibration of hydraulic parameters for large-scale vertical flow constructed wetlands. J. Hydrol. doi:10.1016/j.jhydrol.2009.02.032.

Maji, R., Sudicky, E.A., 2008. Influence of mass transfer characteristics for DNAPL source depletion and contaminant flux in a highly characterized glaciofluvial aquifer. J. Contam. Hydrol. 102 (1–2), 105–119.

Menke, W., 1989. Geophysical Data Analysis: Discrete Inverse Theory. International Geophysics Series 45. Academic Press, Inc., 289 pp.

Poeter, E.P., Mckenna, S.K., 1995. Reducing uncertainty associated with ground-water flow and transport predictions. Ground Water 33 (6), 899–904.

Rubin, Y., Hubbard, S.S., 2005. In: Rubin, Y., Hubbard, S.S. (Eds.), Hydrogeophysics, vol. 523. Springer, Berlin, p. 1-4020-3101-7.

Tarantola, A., 2005. Inverse Problem Theory and Methods for Model Parameter Estimation. SIAM, Philadelphia, PA.

Teutsch, G., Glingbeil, R., Kleineidam, R., 1998. Groundwater quality: remediation and protection, numerical modeling of reactive transport using aquifer analogue data. In: GQ'98: Groundwater Quality Conference, Tübingen, 1998, n250 (Note(s): XII, 598 p.,), pp.381–390. (16 ref.). ISBN: 1-901502-55-4.

Vasco, D.W., Karasaki, K., 2006. Interpretation and inversion of low-frequency head observations. Water Resour. Res. 42, W05408. doi:10.1029/2005WR004445.

Vasco, D.W., Keers, H., Karasaki, K., 2000. Estimation of reservoir properties using transient pressure data: an asymptotic approach. Water Resour. Res. 36 (12), 3447–3465.

Vesselinov, V.V., Neuman, S.P., Illman, W.A., 2001a. Three-dimensional numerical inversion of pneumatic cross-hole tests in unsaturated fractured tuff: 2. Equivalent parameters, high-resolution stochastic imaging and scale effects. Water Resour. Res. 37 (12), 3019–3041.

Vesselinov, V.V., Neuman, S.P., Illman, W.A., 2001b. Three-dimensional numerical inversion of pneumatic cross-hole tests in unsaturated fractured tuff: 1. Methodology. Water Resour. Res. 37 (12), 3001–3017.

Virieux, J., Flores-Luna, C., Gibert, D., 1994. Asymptotic theory for diffusive electromagnetic imaging. Geophys. J. Int. 119, 857–868.

Yeh, T.-C.J., Liu, S., 2000. Hydraulic tomography: development of a new aquifer test method. Water Resour. Res. 36 (8), 2095–2105.

Yin, D., Illman, W.A., 2009. Hydraulic tomography using temporal moments of drawdown recovery data: a laboratory sandbox study. Water Resour. Res. 45, W01502. doi:10.1029/2007WR006623.

Zheng, C., Gorelick, S.M., 2003. Analysis of solute transport in flow fields influenced by preferential flow paths at the decimeter scale. Ground Water 41 (2), 142–155. doi:10.1111/j.1745-6584.2003.tb02578.x.

Zhu, J., Yeh, T.-C.J., 2005. Characterization of aquifer heterogeneity using transient hydraulic tomography. Water Resour. Res. 41, W07028. doi:10.1029/2004WR003790.

Zhu, J., Yeh, T.-C.J., 2006. Analysis of hydraulic tomography using temporal moments of drawdown recovery data. Water Resour. Res. 42, W02403.